Quasi-one-dimensional characters in topological semimetal $TaNiTe_5$

Ni Ma(马妮)[1,2,†], De-Yang Wang(王德阳)[1,2,†], Ben-Rui Huang(黄本锐)[1,2], Kai-Yi Li(李凯仪)[3], Jing-Peng Song(宋靖鹏)[1,2], Jian-Zhong Liu(刘建忠)[1,2], Hong-Ping Mei(梅红萍)[1], Mao Ye(叶茂)[1,2], and Ang Li(李昂)[1,‡]

[1] *State Key Laboratory of Functional Materials for Informatics, Shanghai Institute of Microsystem and Information Technology, Chinese Academy of Sciences, Shanghai* 200050, *China*

[2] *Center of Materials Science and Optoelectronics Engineering, University of Chinese Academy of Sciences, Beijing* 100049, *China*

[3] *School of Physical Science and Technology, ShanghaiTech University, Shanghai* 201210, *China*

(Received 1 September 2022; revised manuscript received 30 October 2022; accepted manuscript online 11 November 2022)

One-dimensional (1D) topological insulators are superior for low-dissipation applications owing to the 1D character of surface states where scatterings other than prohibited backscattering are further restricted. Among the proposed candidates for 1D topological materials, $TaNiTe_5$ has attracted intensive attention for its quasi-one-dimensional (quasi-1D) crystalline structure. In this study, we identify the chain-like construction and anisotropic electronic states on $TaNiTe_5$ surface with scanning tunneling microscopy. The electron scatterings are largely suppressed even with chromium impurities deposited on the surface and magnetic field applied normal to the surface, which endows $TaNiTe_5$ great potential for low-dissipation spintronic applications.

Keywords: quasi-one-dimensional, magnetic impurity, scanning tunneling microscopy

PACS: 68.43.–h, 75.30.Hx, 68.37.Ef **DOI:** 10.1088/1674-1056/aca203

1. Introduction

The topological electronic structures with low-energy quasiparticle excitations have drawn many interests leading to the emergence of abundant new materials,[1–5] especially low-dimensional topological materials. Dimensionality has a powerful influence on physical properties of materials, which manifests as distinct characteristics compared with their common counterparts in higher dimensions. For instance, a two-dimensional (2D) monolayer of bismuth grown on SiC (0001) is characterized as a topological insulator state[6,7] while a quasi-1D bismuthene edge establishes a Tomonaga–Luttinger liquid regime with the separation of charge and spin excitation.[8] The past decades have witnessed mounting investigations of topologically nontrivial surface states in two and three dimensions, whereas 1D topological materials have been rarely identified.

As a new family of topological materials with quasi-1D structural character, layered transition metal tellurides have attracted considerable attention. $TaIrTe_4$[9,10] and $NbIrTe_4$[11] are predicted and verified as topological semimetals, and quasi-1D superconductivity occurs on $TaIrTe_4$ surface.[12] $MM'Te_4$ (M = Nb, Ta; M' = Ir, Rh) composed of alternating Te-based chains hosts classic quasi-1D crystal structure in layered transition metal tellurides.[9,13] Similar anisotropic superconductivity is discovered in the quasi-1D structural analogs $Ta_4Pd_3Te_{16}$[14] and $Ta_3Pd_3Te_{14}$,[15] making the layered transition metal tellurides a promising platform for low-dimensional topological superconductors. Another family in ternary transition metal tellurides, Ta-based $TaMTe_5$ (M = Ni, Pd, Pt),[16–22] as layered 3D topological candidates hosting quasi-1D chains, further enrich the study of low-dimensional topology. The sister compounds $TaNiTe_5$,[16–20] TaPdTe,[21] and $TaPtTe_5$[22] have been experimentally synthesized and their significantly anisotropic features have been validated with magnetization and transport measurements. The de Haas–van Alphen (dHvA) oscillations reveal the nontrivial Berry phases, which provide experimental evidence for the existence of Dirac fermions[23–25] in $TaMTe_5$ (M = Ni, Pd, Pt). Therefore, the nontrivial $TaMTe_5$ (M = Ni, Pd, Pt) with distinctive quasi-1D characteristics may have the potential to be a rational example of the interplay between dimensionality and topological phases.

Such a topological material possesses a nontrivial metallic surface state with spin-momentum locking and chiral spin texture. The linearly dispersed Dirac surface states are well protected against disorders and imperfections due to the time reversal symmetry.[26,27] However, it has been suggested that the gapless Dirac dispersion becomes massive when magnetism is introduced to break the time reversal symmetry. Dirac fermions can mediate the interaction between magnetic impurities via the Ruderman–Kittel–Kasuya–Yosida (RKKY) interaction, resulting in the ordered magnetic moments normal to the surface and therefore a gap opening at the Dirac point.[28–31] Experimentally, the opening of gap in the sur-

†They contributed equally to this work.

‡Corresponding author. E-mail: angli@mail.sim.ac.cn

© 2023 Chinese Physical Society and IOP Publishing Ltd

face state and the consequent quasiparticle backscattering have been observed on the Fe deposited Bi_2Se_3 and Mn deposited Bi_2Te_3 surfaces.[30,31]

In this paper, we use scanning tunneling microscopy/spectroscopy (STM/STS) to characterize the quasi-1D nature of surface atomic and electronic structures in $TaNiTe_5$. Cryogenically cleaved $TaNiTe_5$ is terminated with quasi-1D stripes along the crystallographic a-axis, and the spatial distribution of local density of states (LDOS) exhibits apparent anisotropy. The absence of scattering processes related to the surface bands near Fermi energy is consistent with the spin textures calculated by density functional theory (DFT). The excellent quasi-1D electronic properties may inspire low-dissipation devices and applications.

2. Experimental details

$TaNiTe_5$ single crystals were grown using the self-flux method.[16] Tantalum (99.97%), nickel (99.5%) and tellurium (99.99%) powders in the atomic ratio of 1:1:10 were mixed in an alumina crucible and sealed in a quartz tube under high vacuum. The tube was heated to 1273 K for 24 h and slowly cooled to 773 K at a rate of 5 K/h. Then the quartz tube was removed from the furnace and centrifuged to separate the crystals from the excess Te flux. The needle-like samples were cleaved *in situ* in ultrahigh vacuum (base pressure 6×10^{-11} mbar) at $\sim$ 100 K. In addition to the standard STM samples, the chromium-decorated samples were prepared by electro-beam sputtering on the cleaved samples at 60 K for 10 s. After cleaving or depositing, the crystals were quickly cooled down to 4.5 K for subsequent STM measurements. The electrochemically etched tungsten tips were firstly calibrated on a Cu (100) surface. The topographic images were taken in the constant-current mode and the differential conductance ($\mathrm{d}I/\mathrm{d}V$) spectra were recorded with standard lock-in technique. The frequency and amplitude of excitation signal are 971.0 Hz and 20 mV (10 mV for Fig. 3(a)), respectively. DFT calculations were performed using the Vienna *ab-initio* simulation package.[32–34] Electronic surface states were calculated by constructing localized Wannier functions[35] with the WannierTools package.[36]

3. Results and discussion

3.1. Quasi-1D characters of $TaNiTe_5$

$TaNiTe_5$ has a layered orthorhombic structure (space group *Cmcm*) with lattice constants $a = 3.6675$ Å, $b = 13.172$ Å, $c = 15.142$ Å.[16–20] As shown in Fig. 1(a), the crystal can be viewed as alternating arrays of $TaTe_3$ face-sharing prismatic chains and $NiTe_3$ edge-sharing octahedral chains in the a–c plane and A–A stacked along the b direction.[37] The van der Waals nature of Te–Te interlayer bonding makes the crystal easy to cleave yielding a large area of Te surface. The 1D character of in-plane structure leads to step edges preferentially oriented along the chain (a-axis) direction as shown in Fig. 1(b). The steps are mostly 0.67 nm high, which corresponds to $b/2$. Striped surface structure can be resolved on each terrace and Fig. 1(d) shows the atomic resolution of such a surface. The lattice constants are extracted as $a = 0.36$ nm and $c = 1.5$ nm, in good agreement with the reported values.[16–20] The atomic layout is drawn in Fig. 1(d) according to the mirror symmetry of $TaTe_3$ prismatic chains and the unequal spacing between surface Te atoms. Under the shown bias voltage, the bright rows correspond to the downward $TaTe_3$ prismatic chains where Ta sits at the center of Te rectangle (marked by the black box in Fig. 1(d)) and the dark ones correspond to the upward $TaTe_3$ chains with a diamond Te configuration (the black diamond in Fig. 1(d)).

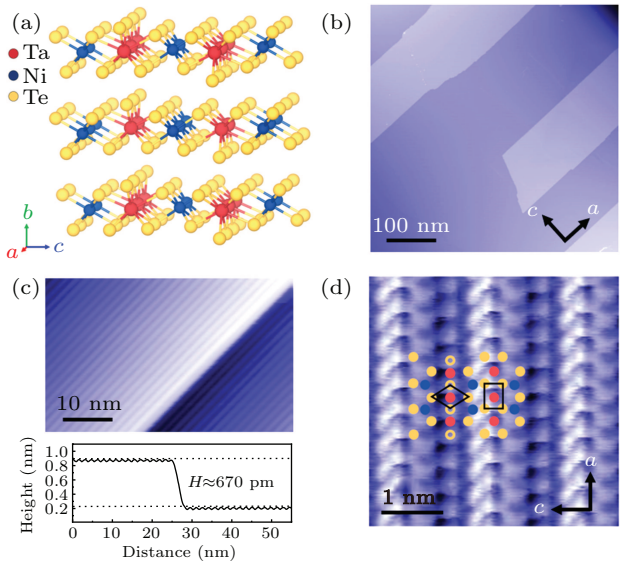


Fig. 1. (a) Crystal structure of $TaNiTe_5$. (b) STM topography of $TaNiTe_5$ surface (500×500 nm^2, sample bias $V = 1.5$ V, tunneling current $I_t = 100$ pA). (c) STM image of the step along a-direction (50×50 nm^2, $V = -1$ V, $I_t = 200$ pA). Lower panel shows the height profile perpendicular to edge. (d) Atomic-resolution image of stripes (4×4 nm^2, $V = -500$ mV, $I_t = 200$ pA). The yellow hollow dots mark apical Te atoms, the yellow solid remaining Te atoms, the red Ta atoms and the blue Ni atoms.

The striped surface shows the topographic contrast reversals as the bias voltage is varied as demonstrated in Fig. 2. It represents the energy dependent spatial variation of integrated DOS hence highlights the electronic contribution in topographic images. The 1D distribution of electronic states is embodied in the crystalline chain-like structure.

The 1D distribution of electronic states creates apparent anisotropy in the low-energy excitations. Typical differential conductance $\mathrm{d}I/\mathrm{d}V$ spectra are shown in Fig. 3(a) for the representative bright (crest) and dark (valley) rows (the downward and upward $TaTe_3$ prismatic chains). The spectra are

similar except for the position of a broad conductance peak between 1 V and 1.5 V. The LDOS exhibits periodic modulation across the stripes (Fig. 3(c)) while it is fairly uniform along the stripes (data not shown). The bulk Brillouin zone (BZ) and its surface projection to the (010) surface (the cleaving plane) are shown in Fig. 3(d). The schematic constant-energy contour based on DFT calculation in Fig. 3(e) shows two surface bands that are topologically nontrivial S_T and trivial S_D, which are experimentally observed by angle-resolved photoemission spectroscopy (ARPES).[19,20] Furthermore, S_T and S_D possess similar spin polarizations in the $\bar{\Gamma}$–$\bar{Z}$ direction according to previous studies.[19,20] The topological surface state S_T is characterized by the helical spin texture that protects the surface electrons from backscattering. Similarly, the spin-selective scattering between S_T and S_D with opposite spins is suppressed. As a result, the scattering vectors in the $\bar{\Gamma}$–$\bar{Z}$ direction, $q_2 \sim q_4$ labelled in Fig. 3(e), are absent in the quasiparticle interference (QPI) pattern, which is dominated by the scatterings between the extremal points on constant-energy contour.[38] Only the inter-band scattering (q_1) between S_T and S_D is allowed although such forward scattering (connects states with parallel velocities) may not necessarily give rise to strong QPI intensities due to destructive interference.[39] The scatterings in the other directions (e.g. $\bar{\Gamma}$–$\bar{X}$ direction) are not permitted either due to their opposite spin polarizations. Accordingly, no quasiparticle scattering is revealed on $TaNiTe_5$ surface by the dI/dV mapping. Essentially only nondispersive stripe modulation can be resolved (~ 0.65 nm^{-1}, marked with red circles in Fig. 3(f)). The quasi-1D transport behavior in $TaNiTe_5$[16–18] further suppresses electron scatterings, which contributes to the good metallicity and long particle lifetime.

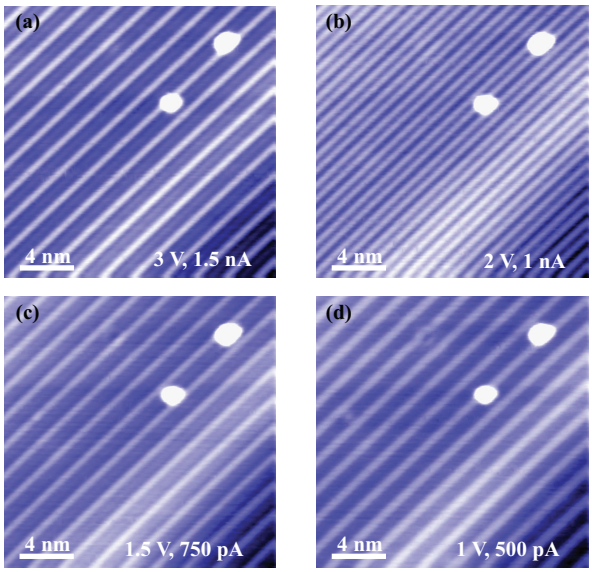


Fig. 2. (a)–(d) Topographic contrast reversals of the same 20×20 nm^2 area at various bias voltages: (a) $V = 3$ V, $I_t = 1.5$ nA; (b) $V = 2$ V, $I_t = 1$ nA; (c) $V = 1.5$ V, $I_t = 750$ pA; (d) $V = 1$ V, $I_t = 500$ pA.

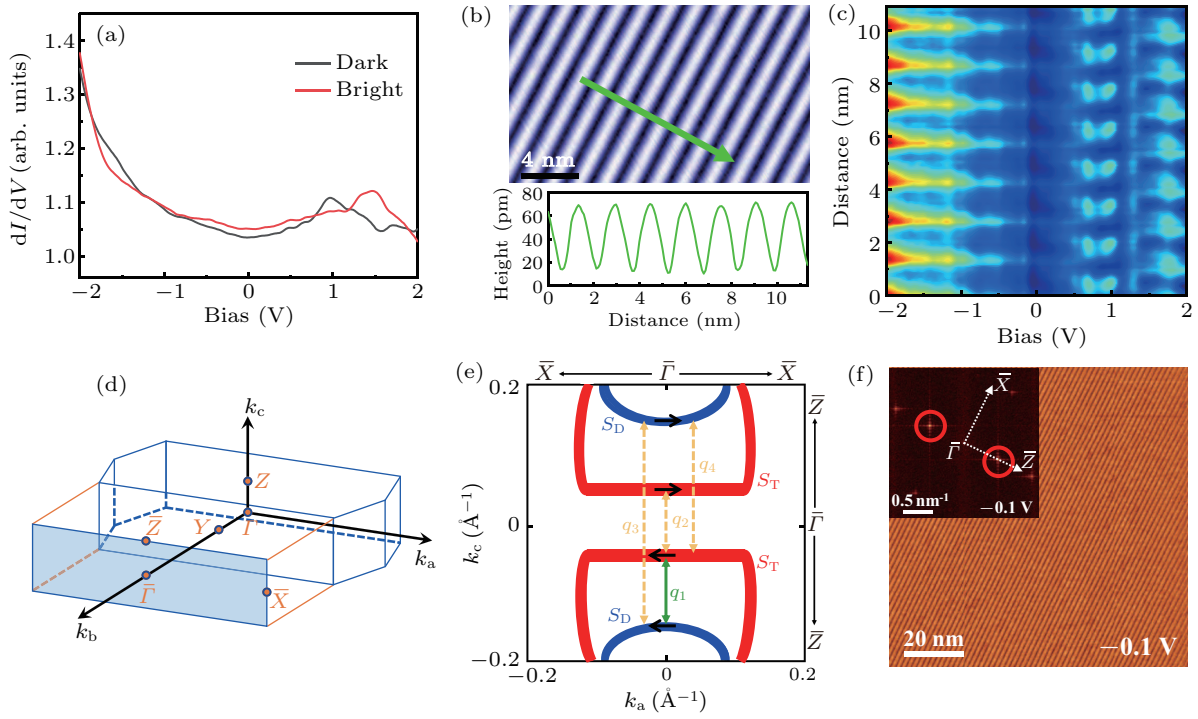


Fig. 3. (a) Typical dI/dV spectra taken on the dark and bright rows (the upward and downward $TaTe_3$ prismatic chain) ($V = -2$ V, $I_t = 200$ pA). (b) STM image of stripes (20×20 nm^2, $V = -200$ mV, $I_t = 200$ pA). Lower panel shows the periodicity of stripes. (c) Typical dI/dV line spectrum ($V = -2$ V, $I_t = 500$ pA) taken along the arrow in (b) perpendicular to stripes. (d) Bulk and surface Brillouin zone with high-symmetry points marked. (e) Schematic of topological and Dirac-like surface bands (S_T and S_D) in the first Brillouin zone at Fermi energy. The spin textures of S_T and S_D along the $\bar{Z}$–$\bar{\Gamma}$–$\bar{Z}$ direction are represented by black arrows. Green and yellow double-head arrows indicate the allowed and forbidden scattering wave vectors. (f) dI/dV mapping of stripes at −0.1 V (100×100 nm^2 with 256×256 pixels, setpoint −0.3 V/1 nA). Inset: corresponding FFT. Red circles mark the 1D stripe modulation.

3.2. Significantly suppressed surface electron scattering

To further explore the electron scattering in low-dimensional topological materials, surface defects are introduced intentionally by depositing chromium adatoms as shown in Fig. 4(a). The Cr adatoms tend to reside on the dark rows (the upward $TaTe_3$ prismatic chains) in the form of single atoms. The typical dI/dV spectrum for such defects is plotted in Fig. 4(b) (black curve), which shows no obvious resonance state except for certain shift in spectral weight. The dI/dV spectrum does not change significantly at negative bias on the Cr adatoms as compared with the ordinary stripe surface. No major scattering vectors, however, can be found in the QPI pattern around the defects (Figs. 4(c) and 4(d)). Basically only the fuzzy background near the zone center coexists with the stripe modulation spots. Apparently the Cr adsorbates neither open the scattering channels nor alter the quasi-1D character of $TaNiTe_5$ surface states. According to the previous ARPES and x-ray magnetic circular dichroism studies,[30,40–42] favorable orientation of magnetic moments may be required to open the Dirac gap. The out-of-plane magnetic moments can induce finite in-plane spin components of electrons.[43,44] The initial k and final-k states are no longer spin-antiparallel under such circumstances thereby allowing the appearance of backscattering vectors.[31]

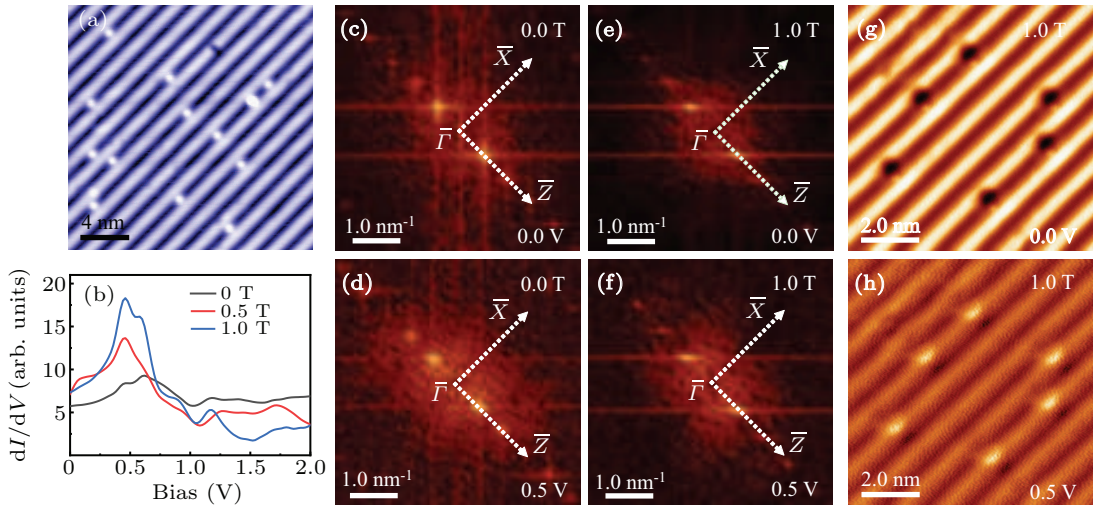


Fig. 4. (a) STM image of Cr-adsorbed $TaNiTe_5$ surface (20×20 nm^2, $V=-1$ V, $I_t=100$ pA). (b) Typical dI/dV spectra ($V=2$ V, $I_t=400$ pA) taken on Cr adatoms under the magnetic field with different magnitudes. (c)–(f) FFT of dI/dV maps obtained on the same Cr absorbed region at (c) 0.0 V/0.0 T, (d) 0.5 V/0.0 T, (e) 0.0 V/1.0 T, (f) 0.5 V/1.0 T, respectively. (g)–(h) Real space dI/dV maps corresponding to (e)–(f) (12×12 nm^2 with 256×256 pixels, setpoint $+1$ V/2 nA).

An external magnetic field is applied perpendicular to the sample surface up to 1 T. In Fig. 4(b), the LDOS peak(s) around 0.5 V grows with the field. Nevertheless, no standing waves can be recognized in the vicinity of Cr impurities (Figs. 4(e)–4(h)) indicating that S_T is preserved. The reason could be: (1) the magnetic field in our experiment is unable to switch the Cr moments; or (2) either the magnetic moments of Cr or the Cr induced magnetization in $TaNiTe_5$ is too weak.[42,43] Nevertheless, the suppressed scatterings of surface states persist in the presence of Cr surface doping and external magnetic field.

4. Conclusion

In summary, we have identified the quasi-one dimensional atomic and electronic structures on cleaved $TaNiTe_5$ surface. Low-energy electron scatterings are significantly suppressed on such surfaces due to the protection not only from band topology but also from one dimensionality. Such a property may present $TaNiTe_5$ and similar materials with potential applications as low-dissipation devices.

Acknowledgements

Project supported by the National Key R&D Program of China (Grant No. 2017YFA0305400) and the National Natural Science Foundation of China (Grant No. 11227902).

References

[1] Hasan M Z and Kane C L 2010 *Rev. Mod. Phys.* **82** 3045
[2] Armitage N P, Mele E J and Vishwanath A 2018 *Rev. Mod. Phys.* **90** 015001
[3] Burkov A A 2016 *Nat. Mater.* **15** 1145
[4] Yan B and Felser C 2017 *Annu. Rev. Condens. Matter Phys.* **8** 337
[5] Nagaosa N, Morimoto T and Tokura Y 2020 *Nat. Rev. Mater.* **5** 621
[6] Reis F, Li G, Dudy L, Bauernfeind M, Glass S, Hanke W, Thomale R, Schäfer J and Claessen R 2017 *Science* **357** 287
[7] Li G, Hanke W, Hankiewicz E M, Reis F, Schäfer J, Claessen R, Wu C and Thomale R 2018 *Phys. Rev. B* **98** 165146
[8] Stühler R, Reis F, Müller T, Helbig T, Schwemmer T, Thomale R, Schäfer J and Claessen R 2020 *Nat. Phys.* **16** 47
[9] Koepernik K, Kasinathan D, Efremov D V, Khim S, Borisenko S, Büchner B and van den Brink J 2016 *Phys. Rev. B* **93** 201101
[10] Khim S, Koepernik K, Efremov D V, Klotz J, Förster T, Wosnitza J, Sturza M I, Wurmehl S, Hess C, van den Brink J and Büchner B 2016 *Phys. Rev. B* **94** 165145
[11] Zhou W, Li B, Xu C Q, van Delft M R, Chen Y G, Fan X C, Qian B, Hussey N E and Xu X F 2019 *Adv. Electron. Mater.* **5** 1900250

[12] Xing Y, Shao Z B, Ge J, Luo J W, Wang J H, Zhu Z W, Liu J, Wang Y, Zhao Z Y, Yan J Q, Mandrus D, Yan B H, Liu X J, Pan M H and Wang J 2020 *Natl. Sci. Rev.* **7** 579

[13] Liu J W, Wang H, Fang C, Fu L and Qian X F 2017 *Nano Lett.* **17** 467

[14] Jiao W H, Tang Z T, Sun Y L, Liu Y, Tao Q, Feng C M, Zeng Y W, Xu Z A and Cao G H 2014 *J. Am. Chem. Soc.* **136** 1284

[15] Jiao W H, He L P, Liu Y, Xu X F, Li Y K, Zhang C H, Zhou N, Xu Z A, Li S Y and Cao G H 2016 *Sci. Rep.* **6** 21628

[16] Xu C Q, Liu Y, Cai P G, Li B, Jiao W H, Li Y L, Zhang J Y, Zhou W, Qian B, Jiang X F, Shi Z X, Sankar R, Zhang J L, Yang F, Zhu Z W, Biswas P, Qian D, Ke X L and Xu X F 2020 *J. Phys. Chem. Lett.* **11** 7782

[17] Chen Z, Wu M, Zhang Y, Zhang J L, Nie Y, Qin Y L, Han Y Y, Xi C Y, Ma S Q, Kan X C, Zhou J H, Yang X P, Zhu X D, Ning W and Tian M L 2021 *Phys. Rev. B* **103** 035105

[18] Hao Z Y, Chen W Z, Wang Y, *et al* 2021 *Phys. Rev. B* **104** 115158

[19] Li Y L, Ran Z, Huang C Z, *et al* 2022 *Phys. Rev. Lett.* **128** 106802

[20] Wang D Y, Jiang Q, Kuroda K, Kawaguchi K, Harasawa A, Yaji K, Ernst A, Qian H J, Liu W J, Zha H M, Jiang Z C, Ma N, Mei H P, Li A, Kondo T, Qiao S and Ye M 2022 *Phys. Rev. Lett.* **129** 146401

[21] Jiao W H, Xie X M, Liu Y, Xu X F, Li B, Xu C Q, Liu J Y, Zhou W, Li Y K, Yang H Y, Jiang S, Luo Y K, Zhu Z W and Cao G H 2020 *Phys. Rev. B* **102** 075141

[22] Jiao W H, Xiao S Z, Li B, Xu C Q, Xie X M, Qiu H Q, Xu X F, Liu Y, Song S J, Zhou W, Zhai H F, Ke X, He S L and Cao G H 2021 *Phys. Rev. B* **103** 125150

[23] Murakawa H, Bahramy M S, Tokunaga M, Kohama Y, Bell C, Kaneko Y, Nagaosa N, Hwang H Y and Tokura Y 2013 *Science* **342** 1490

[24] He L P, Hong X C, Dong J K, Pan J, Zhang Z, Zhang J and Li S Y 2014 *Phys. Rev. Lett.* **113** 246402

[25] Gao W S, Hao N N, Zheng F W, Ning W, Wu M, Zhu X D, Zheng G L, Zhang J L, Lu J W, Zhang H W, Xi C Y, Yang J Y, Du H F, Zhang P, Zhang Y H and Tian M L 2017 *Phys. Rev. Lett.* **118** 256601

[26] Ando Y and Fu L 2015 *Annu. Rev. Condens. Matter Phys.* **6** 361

[27] Roushan P, Seo J, Parker C V, Hor Y S, Hsieh D, Qian D, Richardella A, Hasan M Z, Cava R J and Yazdani A 2009 *Nature* **460** 1106

[28] Hor Y S, Roushan P, Beidenkopf H, Seo J, Qu D, Checkelsky J G, Wray L A, Hsieh D, Xia Y, Xu S Y, Qian D, Hasan M Z, Ong N P, Yazdani A and Cava R J 2010 *Phys. Rev. B* **81** 195203

[29] Chen Y L, Chu J H, Analytis J G, Liu Z K, Igarashi K, Kuo H H, Qi X L, Mo S K, Moore R G, Lu D H, Hashimoto M, Sasagawa T, Zhang S C, Fisher I R, Hussain Z and Shen Z X 2010 *Science* **329** 659

[30] Wray L A, Xu S Y, Xia Y Q, Hsieh D, Fedorov A V, Hor Y S, Cava R J, Bansil A, Lin H and Hasan M Z 2011 *Nat. Phys.* **7** 32

[31] Sessi P, Reis F, Bathon T, Kokh K A, Tereshchenko O E and Bode M 2014 *Nat. Commun.* **5** 5349

[32] Kresse G and Hafner J 1993 *Phys. Rev. B* **47** 558

[33] Kresse G and Furthmüller J 1996 *Phys. Rev. B* **54** 11169

[34] Kresse G and Joubert D 1999 *Phys. Rev. B* **59** 1758

[35] Mostofi A A, Yates J R, Lee Y S, Souza I, Vanderbilt D and Marzari N 2008 *Comput. Phys. Commun.* **178** 685

[36] Wu Q S, Zhang S N, Song H F, Troyer M and Soluyanov A A 2018 *Comput. Phys. Commun.* **224** 405

[37] Alemany P and Canadell E 1999 *Eur. J. Inorg. Chem.* **1999** 1701

[38] Wang J, Li W, Cheng P, Song C, Zhang T, Deng P, Chen X, Ma X C, He K, Jia J F, Xue Q K and Zhu B F 2011 *Phys. Rev. B* **84** 235447

[39] Jolie W, Lux J, Pörtner M, Dombrowski D, Herbig C, Knispel T, Simon S, Michely T, Rosch A and Busse C 2018 *Phys. Rev. Lett.* **120** 106801

[40] Honolka J, Khajetoorians A A, Sessi V, Wehling T O, Stepanow S, Mi J L, Iversen B B, Schlenk T, Wiebe J, Brookes N B, Lichtenstein A I, Hofmann P, Kern K and Wiesendanger R 2012 *Phys. Rev. Lett.* **108** 256811

[41] Shelford L R, Hesjedal T, Collins-McIntyre L, Dhesi S S, Maccherozzi F and van der Laan G 2012 *Phys. Rev. B* **86** 081304

[42] Ye M, Eremeev S V, Kuroda K, Krasovskii E E, Chulkov E V, Takeda Y, Saitoh Y, Okamoto K, Zhu S Y, Miyamoto K, Arita M, Nakatake M, Okuda T, Ueda Y, Shimada K, Namatame H, Taniguchi M and Kimura A 2012 *Phys. Rev. B* **85** 205317

[43] Liu Q, Liu C X, Xu C K, Qi X L and Zhang S C 2009 *Phys. Rev. Lett.* **102** 156603

[44] Biswas R R and Balatsky A V 2010 *Phys. Rev. B* **81** 233405